

Generation of Hyperentangled Photon Pairs

Julio T. Barreiro,¹ Nathan K. Langford,² Nicholas A. Peters,¹ and Paul G. Kwiat¹

¹*Department of Physics, University of Illinois at Urbana-Champaign, Urbana, IL 61801-3080, USA*

²*Department of Physics, University of Queensland, Brisbane, QLD 4072, Australia*

(Dated: October 29, 2018)

We experimentally demonstrate the first quantum system entangled in *every* degree of freedom (hyperentangled). Using pairs of photons produced in spontaneous parametric down-conversion, we verify entanglement by observing a Bell-type inequality violation in each degree of freedom: polarization, spatial mode and time-energy. We also produce and characterize maximally hyperentangled states and novel states simultaneously exhibiting both quantum and classical correlations. Finally, we report the tomography of a $2 \times 2 \times 3 \times 3$ system (36-dimensional Hilbert space), which we believe is the first reported photonic entangled system of this size to be so characterized.

PACS numbers: 03.65.Ud, 42.50.Dv, 03.67.Mn, 42.65.Lm

Entanglement, the quintessential quantum mechanical correlations that can exist between quantum systems, plays a critical role in many important applications in quantum information processing, including the revolutionary one-way quantum computer [1], quantum cryptography [2], dense coding [3] and teleportation [4]. As a result, the ability to create, control and manipulate entanglement has been a defining experimental goal in recent years. Higher-order entanglement has been realized in multi-particle [5] and multi-dimensional [6, 7, 8, 9] systems. Furthermore, two-component quantum systems can be entangled in every degree of freedom (DOF), or hyperentangled [10]. These systems enable the implementation of 100%-efficient complete Bell-state analysis with only linear elements [11] and techniques for state purification [12]. In addition, hyperentanglement can also be interpreted as entanglement between two higher-dimensional quantum systems, offering significant advantages in quantum communication protocols (e.g., secure superdense coding [13] and cryptography [14]).

Photon pairs produced via the nonlinear optical process of spontaneous parametric down-conversion have many accessible DOF which can be exploited for the production of entanglement. This was first demonstrated using polarization [15, 16], but the list expanded rapidly to include momentum (linear [17], orbital [6], and transverse [18] spatial modes), energy-time [19] and time-bin [20], simultaneous polarization and energy-time [21], and recently, simultaneous polarization and 2-level linear momentum [22]. In this work, we produce and characterize pairs of single photons simultaneously entangled in *every* DOF –polarization, spatial mode and energy-time. As observed previously [6], photon pairs from a *single* nonlinear crystal are entangled in orbital angular momentum (OAM). Moreover, polarization entangled states can be created by coherently pumping *two* contiguous thin crystals [23], provided the spatial modes emitted from each crystal are indistinguishable. Finally, the pump distributes energy to the daughter photons in many ways, entangling each pair in energy; equivalently, each pair

is coherently emitted over a range of times (within the coherence of the continuous wave pump). We show our two-crystal source can generate a $2 \times 2 \times 3 \times 3 \times 2$ -dimensional hyperentangled state [10], approximately

$$\underbrace{(|HH\rangle + |VV\rangle)}_{\text{polarization}} \otimes \underbrace{(|rl\rangle + \alpha|gg\rangle + |lr\rangle)}_{\text{spatial modes}} \otimes \underbrace{(|ss\rangle + |ff\rangle)}_{\text{energy-time}}. \quad (1)$$

Here H (V) represents the horizontal (vertical) photon polarization; $|l\rangle$, $|g\rangle$ and $|r\rangle$, represent the paraxial spatial modes (Laguerre-Gauss) carrying $-\hbar$, 0 , and $+\hbar$ OAM, respectively [24]; α describes the OAM spatial mode balance prescribed by the source [25] and selected via the mode-matching conditions; and $|s\rangle$ and $|f\rangle$, respectively, represent the relative early and late emission times of a pair of energy anticorrelated photons [19].

The most common maximally entangled states are the 2-qubit Bell states: $\Phi^\pm = (|00\rangle \pm |11\rangle)/\sqrt{2}$ and $\Psi^\pm = (|01\rangle \pm |10\rangle)/\sqrt{2}$, in the logical basis $|0\rangle$ and $|1\rangle$. By collecting only the $\pm\hbar$ OAM state of the spatial subspace, the state (1) becomes a tensor product of three Bell states $\Phi_{\text{poln}}^+ \otimes \Phi_{\text{spa}}^+ \otimes \Phi_{\text{t-e}}^+$. As a preliminary test of the hyperentanglement, we characterized the polarization and spatial mode subspaces by measuring the entanglement (characterized by tangle T [26]), the mixture (characterized by linear entropy $S_L(\rho) = \frac{4}{3}[1 - \text{Tr}(\rho^2)]$ [27]), and the fidelity $F(\rho, \rho_t) \equiv (\text{Tr}(\sqrt{\sqrt{\rho_t}\rho\sqrt{\rho_t}}))^2$ of the measured state ρ with the target state $\rho_t = |\psi_t\rangle\langle\psi_t|$. We consistently measured high-quality states with tangles, linear entropies, and fidelities with Φ^+ of $T = 0.99(1)$, $S_L = 0.01(1)$ and $F = 0.99(1)$ for polarization; and $T = 0.96(1)$, $S_L = 0.03(1)$ and $F = 0.95(1)$ for spatial mode, significantly higher than earlier results [18]. The experiment is illustrated in Fig. 1. A 120-mW 351-nm Ar^+ laser pumps two contiguous β -barium borate (BBO) nonlinear crystals with optic axes aligned in perpendicular planes [23]. Each 0.6-mm thick crystal is phase-matched to produce Type-I degenerate photons at 702 nm into a cone of 3.0° half-opening angle. The first (second) crystal produce pairs of horizontally (vertically) po-

larized photons and these two possible down-conversion processes are coherent, provided the spatial modes emitted from each crystal are indistinguishable. With the pump focused to a waist at the crystals, this constraint can be satisfied by using thin crystals and “large” beam waists (large relative to the mismatch in the overlap of the down-conversion cones from each crystal [23]). However, the OAM-entanglement is maximized by balancing the relative populations of the low-valued OAM eigenstates [25], which requires smaller beam waists to image a large area of the down-conversion cones. Here we compromise by employing an intermediate waist size ($\sim 90 \mu\text{m}$) at the crystal. Mode-matching lenses are then used to optimize the coupling of the rapidly diverging down-conversion modes into single-mode collection fibers.

The measurement process consists of three stages of local state projection, one for each DOF. At each stage, the target state is transformed into a state that can be discriminated from the other states with high accuracy. Specifically, computer-generated phase holograms [28] transform the target spatial mode into the pure gaussian (or 0-OAM) mode, which is then filtered by the single-mode fiber [6] (Fig. 1b). After a polarization controller to compensate for the fiber birefringence, wave plates transform the target polarization state into horizontal, which is filtered by a polarizer (Fig. 1d). The analysis of the energy-time state is realized by a Franson-type [19] polarization interferometer without detection post-selection [21]. The matched unbalanced interferometers give each photon a fast $|f\rangle$ and slow $|s\rangle$ route to its detector. Our interferometers consisted of $L \sim 11\text{-mm}$ quartz birefringent elements, which longitudinally separated the horizontal and vertical polarization components by $\Delta n_{\text{quartz}}L \sim 100 \mu\text{m}$, more than the single-photon coherence length ($\lambda^2/\Delta\lambda \sim$

$50 \mu\text{m}$ with $\Delta\lambda = 10 \text{ nm}$ from the interference filters) but much less than the pump-photon coherence length ($\sim 10 \text{ cm}$). We rely on the photons’ polarization entanglement $|HH\rangle + |VV\rangle$ to thus project onto a two-time state ($|Hs, Hs\rangle + e^{i(\delta_1+\delta_2)}|Vf, Vf\rangle$), where δ_1 and δ_2 are controlled by birefringent elements (liquid crystals and quarter-wave plates) in the path of each photon [21]. Finally, by analyzing the polarization in the $\pm 45^\circ$ basis, we erase the distinguishing polarization labels and can directly measure the coherence between the $|ss\rangle$ and $|ff\rangle$ terms, arising from the energy-time entanglement.

To verify quantum mechanical correlations, we tested every DOF against a Clauser-Horne-Shimony-Holt (CHSH) Bell inequality [29]. The CHSH inequality places constraints ($S \leq 2$) on the value of the Bell parameter S , a combination of four two-particle correlation probabilities using two possible analysis settings for each photon. If $S > 2$, no separable quantum system (or local hidden variable theory) can explain the correlations; in this sense, a Bell inequality acts as an “entanglement witness” [30]. To measure the strongest violation for the polarization and spatial-mode DOFs, we determined the optimal measurement settings by first tomographically reconstructing the 2-qubit subspace of interest; we employ a maximum likelihood technique to identify the density matrix most consistent with the data [27].

Table I shows the Bell parameters measured for the polarization, spatial mode, and energy-time subspaces, with various projections in the complementary DOF. We see that for every subspace, the Bell parameter exceeded the classical limit of $S = 2$ by more than 20 standard deviations (σ), verifying the hyperentanglement. For both the polarization and spatial-mode measurements, we traced over the energy-time DOF by not projecting in this subspace. We measured the polarization correlations while projecting the spatial modes into the orthogonal basis states ($|l\rangle, |g\rangle$, and $|r\rangle$), as well as the superpositions $|h\rangle \equiv (|l\rangle + |r\rangle)/\sqrt{2}$ and $|v\rangle \equiv (|l\rangle - |r\rangle)/\sqrt{2}$. The measured Bell parameters agreed (within $\sim 2\sigma$) with predictions from tomographic reconstruction and violated the

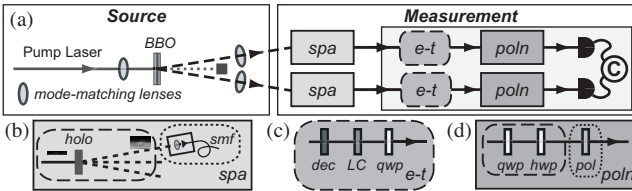


FIG. 1: Experimental setup for the creation and analysis of hyperentangled photons. (a) The photons, produced using adjacent nonlinear crystals (BBO), pass through a state filtration process for each DOF before coincidence detection. The measurement insets show the filtration processes as a transformation of the target state (dashed box) and a filtering step to discard the other components of the state (dotted box). (b) *Spatial Filtration (spa)*: hologram (holo) and single-mode fiber (smf). (c) *Energy-Time Transformation (e-t)*: thick quartz decoherer (dec) and liquid crystal (LC). (d) *Polarization Filtration (poln)*: quarter-wave plate (qwp), half-wave plate (hwp) and polarizer (pol).

TABLE I: Bell parameter S showing CHSH-Bell inequality violations in every degree of freedom. The local realistic limit ($S \leq 2$) is violated by the number of standard deviations shown in brackets, determined by counting statistics.

| DOF | Spatial mode projected subspaces | | | | |
|---------------------------------|---|-------------------------|-------------------------|-------------------------|-------------------------|
| | $ gg\rangle\langle gg $ | $ rl\rangle\langle rl $ | $ lr\rangle\langle lr $ | $ hh\rangle\langle hh $ | $ vv\rangle\langle vv $ |
| Φ_{poln}^+ | 2.76[76 σ] | 2.78[46 σ] | 2.75[44 σ] | 2.81[40 σ] | 2.75[33 σ] |
| $\Phi_{\text{e-t}}^+$ | 2.78[77 σ] | 2.80[40 σ] | 2.80[40 σ] | 2.72[30 σ] | 2.74[29 σ] |
| DOF | Polarization projected subspaces | | | | |
| | no polarizers $ HH\rangle\langle HH $ $ VV\rangle\langle VV $ | | | | |
| Φ_{spa}^+ | 2.78[78 σ] | 2.80[36 σ] | 2.79[37 σ] | | |
| $\alpha gg\rangle + rl\rangle$ | 2.33[55 σ] | 2.30[25 σ] | 2.38[30 σ] | | |
| $\alpha gg\rangle + lr\rangle$ | 2.28[47 σ] | 2.26[20 σ] | 2.31[26 σ] | | |

inequality by more than 30σ . In the spatial mode DOF, the correlations for the state Φ_{spa}^+ were close to maximal ($S = 2\sqrt{2} \approx 2.83$), also in agreement with predictions from the measured state density matrix. In addition, we tested Bell inequalities for non-maximally entangled states in the OAM-subspace: $\alpha|gg\rangle + |rl\rangle$ and $\alpha|gg\rangle + |lr\rangle$; the measured Bell parameters in this case were slightly smaller (5%, max.) than predictions from tomographic reconstruction [31], yet still 20σ above the classical limit. Finally, our measured Bell violation for the energy-time DOF using particular phase settings is in good agreement with the prediction ($S = 2\sqrt{2}V$) from the measured 2-photon interference visibility $V = 0.985(2)$.

The polarization and spatial-mode state was fully characterized via tomography [27]. We performed the 1296 linearly independent state projections required for a full reconstruction in the $(2 \otimes 3) \otimes (2 \otimes 3)$ Hilbert space consisting of two polarization and three OAM modes for each photon. The measured state (Fig. 2) overlaps the anticipated state (polarization and spatial DOFs of Eq. 1) with a fidelity of $0.69(1)$ for $\alpha = 1.88e^{0.16i\pi}$ (numerically fitted), and $S_L = 0.46(1)$, suggesting the difference arises mostly from mixture. Treating the photon pairs as a six-level two-particle system, we can quantify the entanglement using the negativity N [33]. In this $6 \otimes 6$ Hilbert

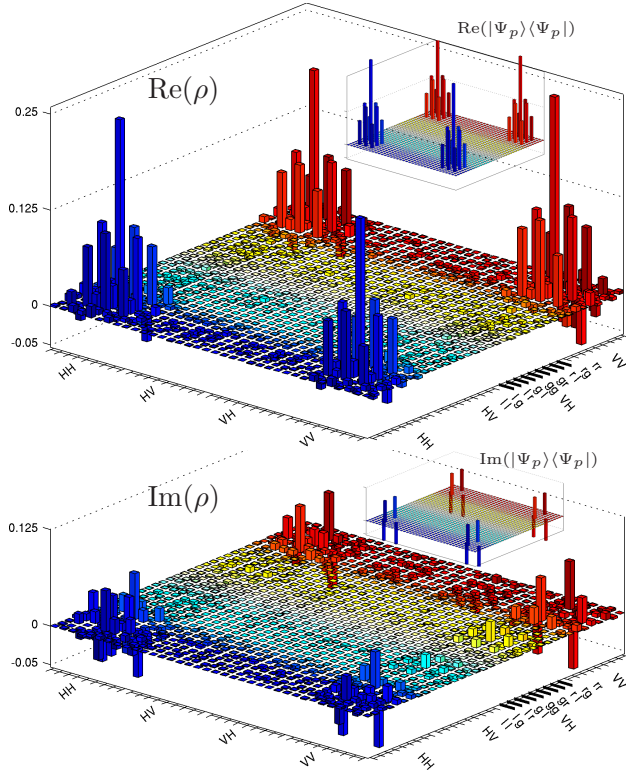


FIG. 2: (color online). Measured density matrix (ρ) and close pure state ($|\Psi_p\rangle \sim \Phi_{\text{poln}}^+ \otimes (|lr\rangle + \alpha|gg\rangle + |rl\rangle)$ with $\alpha = 1.88e^{0.16i\pi}$) of a $(2 \times 2 \times 3)$ -dimensional state of 2-photon polarization and spatial mode [32].

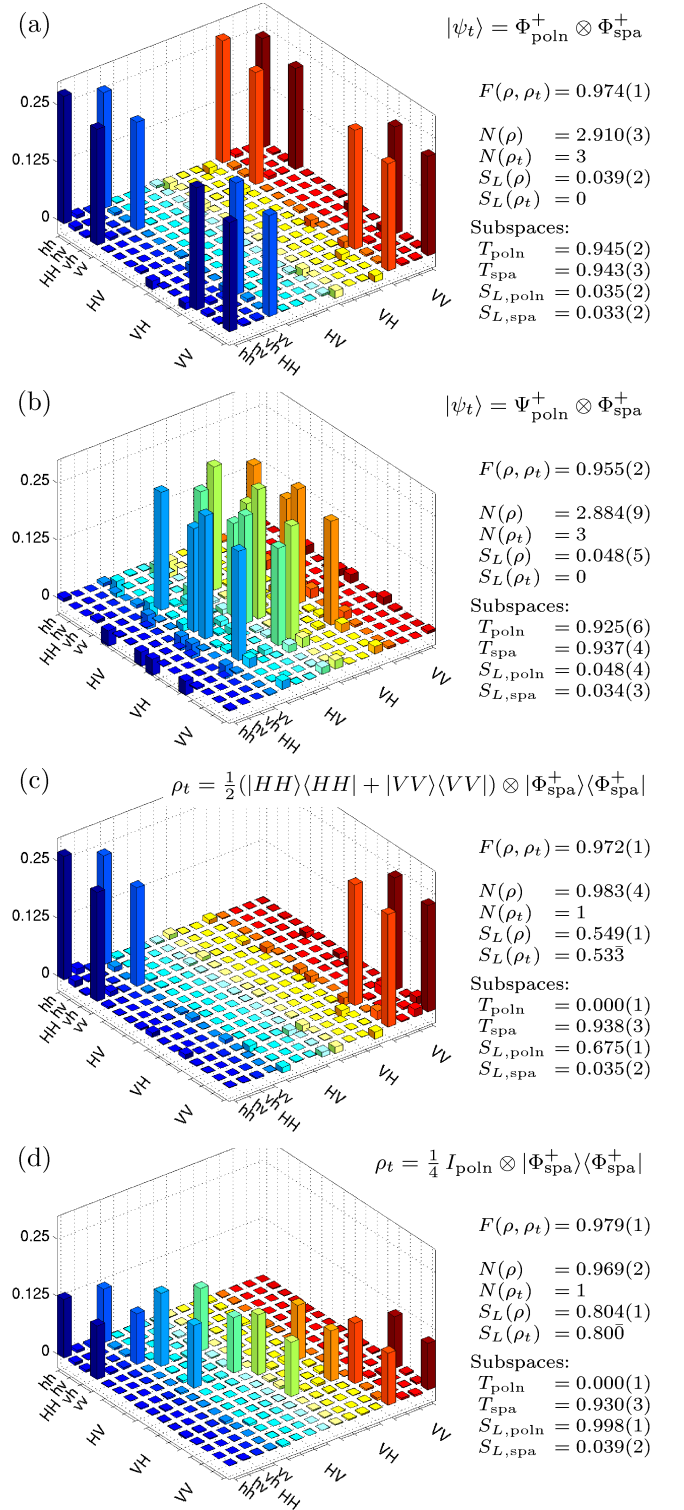


FIG. 3: (color online). Measured density matrices (real parts) of $(2 \times 2 \times 2)$ -dimensional states of 2-photon polarization and $(+1, -1)$ -qubit OAM [32]. For each state, we list: the target state ρ_t , the fidelity $F(\rho, \rho_t)$ of the measured state ρ with the target ρ_t , their negativities and linear entropies, and the tangle and linear entropy for each subspace. The negativity for two-qubit states is the square root of the tangle. The magnitudes of all imaginary elements, not shown, are less than 0.03.

space, N ranges from 0 (for separable states) to 5 (for maximally-entangled states), and the fitted state above has $N \approx 4.44$. Our measured partially mixed state has $N = 2.96(4)$, indicating strong entanglement. The spatial mode alone has $N = 1.14(2)$, greater than the maximum ($N = 1$) of any two-qubit system. Thus, our large state possesses 2-qubit and 2-qutrit entanglement.

We also selected a state (neglecting the $|gg\rangle$ component, Fig. 3a) maximally entangled in both polarization and spatial mode, that had $F = 0.974(1)$ with the target $\Phi_{\text{poln}}^+ \otimes \Phi_{\text{spa}}^+$. By tracing over polarization (spatial mode), we look at the measured state in the spatial mode (polarization) subspaces. The reduced states in both DOFs are pure ($S_L < 0.04$) and highly entangled ($T > 0.94$).

With this precise source of hyperentanglement, we have the flexibility to prepare nearly arbitrary polarization states [34], and to select arbitrary spatial-mode encodings. For example, we also generated a different maximally entangled state: $\Psi_{\text{poln}}^+ \otimes \Phi_{\text{spa}}^+$ (Fig. 3b). By coupling to and tracing over the energy-time DOF using quartz decoherers [34], we can add mixture to the polarization subspace, allowing us to prepare a previously unrealized state that simultaneously displays *classical correlations* in polarization and maximal *quantum correlations* between spatial modes (Fig. 3c): $\rho \approx \frac{1}{2}(|HH\rangle\langle HH| + |VV\rangle\langle VV|) \otimes |\Phi_{\text{spa}}^+\rangle\langle\Phi_{\text{spa}}^+|$. We were also able to accurately prepare the state $\rho_t = \frac{1}{4}I_{\text{poln}} \otimes |\Phi_{\text{spa}}^+\rangle\langle\Phi_{\text{spa}}^+|$, with no polarization correlations at all (i.e., completely mixed or unpolarized), while still maintaining near maximal entanglement in the spatial DOF (Fig. 3d).

We report the first realization of hyperentanglement of a pair of single photons. The entanglement in each DOF is demonstrated by violations of CHSH-Bell inequalities of greater than 20σ . Also, using tomography we fully characterize a $2 \otimes 2 \otimes 3 \otimes 3$ state, the largest quantum system to date. In restricted ($2 \times 2 \times 2 \times 2$)-dimensional subspace, we prepare a range of target states with unprecedented fidelities for quantum systems of this size, including novel states with a controllable degree of correlation in the polarization subspace. These hyperentangled states enable 100%-efficient Bell-state analysis [11], which is important for a variety of quantum information protocols [3, 13]. Because the spatial mode and energy-time DOFs are infinite in size, we envision examining even larger subspaces, encoding higher-dimensional qudits [7, 8]. Finally, we note that the pairwise mechanism of the $\chi^{(2)}$ down-conversion process inherently produces entanglement in photon number [35].

We thank A. G. White and T.-C. Wei for helpful discussions and the ARO/ARDA-sponsored MURI Center for Photonic Quantum Information Systems, the ARC, and the U. Queensland Found. for support. J.T.B. acknowledges support from CONACYT-México.

-
- [1] R. Raussendorf and H. J. Briegel, Phys. Rev. Lett. **86**, 5188 (2001).
 - [2] A. K. Ekert, Phys. Rev. Lett. **67**, 661 (1991).
 - [3] C. H. Bennett and S. J. Wiesner, Phys. Rev. Lett. **69**, 2881 (1992).
 - [4] C. H. Bennett et al., Phys. Rev. Lett. **70**, 1895 (1993).
 - [5] Z. Zhao et al., Nature **430**, 54 (2004); P. Walther et al., Nature **434**, 169 (2005).
 - [6] A. Mair, A. Vaziri, G. Weihs, and A. Zeilinger, Nature **412**, 313 (2001).
 - [7] R. T. Thew, A. Acín, H. Zbinden, and N. Gisin, Phys. Rev. Lett. **93**, 10503 (2004).
 - [8] M. N. OSullivan-Hale, I. A. Khan, R. W. Boyd, and J. C. Howell, Phys. Rev. Lett. **94**, 220501 (2005).
 - [9] S. Oemrawsingh et al., Phys. Rev. Lett. **95**, 240501 (2005).
 - [10] P. G. Kwiat, J. Mod. Opt. **44**, 2173 (1997).
 - [11] P. G. Kwiat and H. Weinfurter, Phys. Rev. A **58**, R2623 (1998).
 - [12] C. Simon and J.-W. Pan, Phys. Rev. Lett. **89**, 257901 (2002).
 - [13] C. Wang et al., Phys. Rev. A **71**, 044305 (2005).
 - [14] D. Bruss and C. Macchiavello, Phys. Rev. Lett. **88**, 127901 (2002); N. J. Cerf, M. Bourennane, A. Karlsson, and N. Gisin, Phys. Rev. Lett. **88**, 127902 (2002).
 - [15] Z. Y. Ou and L. Mandel, Phys. Rev. Lett. **61**, 50 (1988).
 - [16] Y. H. Shih and C. O. Alley, Phys. Rev. Lett. **61**, 2921 (1988).
 - [17] J. G. Rarity and P. R. Tapster, Phys. Rev. Lett. **64**, 2495 (1990).
 - [18] N. Langford et al., Phys. Rev. Lett. **93**, 53601 (2004).
 - [19] J. D. Franson, Phys. Rev. Lett. **62**, 2205 (1989).
 - [20] J. Brendel, N. Gisin, W. Tittel, and H. Zbinden, Phys. Rev. Lett. **82**, 2594 (1999).
 - [21] D. V. Strekalov et al., Phys. Rev. A **54**, R1 (1996).
 - [22] T. Yang et al., Phys. Rev. Lett. **95**, 240406 (2005); C. Cinelli et al., Phys. Rev. Lett. **95**, 240405 (2005).
 - [23] P. G. Kwiat et al., Phys. Rev. A **60**, R773 (1999).
 - [24] L. Allen, S. M. Barnett, and M. J. Padgett, eds., *Optical Angular Momentum* (IoP Publishing, Bristol, 2003).
 - [25] J. P. Torres, A. Alexandrescu, and L. Torner, Phys. Rev. A **68**, 050301 (2003).
 - [26] W. K. Wootters, Phys. Rev. Lett. **80**, 2245 (1998); $T(\rho) = [\max\{0, \lambda_1 - \lambda_2 - \lambda_3 - \lambda_4\}]^2$, λ_i are the square roots of the eigenvalues of $\rho(\sigma_2 \otimes \sigma_2)\rho^*(\sigma_2 \otimes \sigma_2)$ in non-increasing order by magnitude, with $\sigma_2 = \begin{pmatrix} 0 & -i \\ i & 0 \end{pmatrix}$.
 - [27] D. F. V. James, P. G. Kwiat, W. J. Munro, and A. G. White, Phys. Rev. A **64**, 052312 (2001).
 - [28] Binary plane-wave phase gratings [24] ($\sim 40\%$ diffraction efficiency) project the states $|g\rangle, |l\rangle, |r\rangle$ and $\cos(\theta)|h\rangle + \sin(\theta)|v\rangle = |l\rangle + e^{i2\theta}|r\rangle$ with $\theta = n\pi/8, n = -1, 0, \dots, 8$. By displacing the holograms for $|l\rangle$ ($|r\rangle$) we project arbitrary linear combinations [6] of $|g\rangle$ and $|l\rangle$ ($|r\rangle$).
 - [29] J. Clauser, M. A. Horne, A. Shimony, and R. A. Holt, Phys. Rev. Lett. **23**, 880 (1969).
 - [30] B. M. Terhal, Phys. Lett. A **271**, 319 (2000).
 - [31] Displaced plane-wave holograms allow small leakage of unwanted states into the fiber [18]. This potentially explains the smaller-than-predicted Bell parameter for the non-maximally entangled spatial-mode states (e.g., $S_{\text{exp}} = 2.28(1)$ versus the prediction $S_{\text{pred}} = 2.35$).

- [32] Data in Fig. 2 (Fig. 3) were collected for 40 s (20 s) per projection with ~ 600 (~ 100) detected pairs/s.
- [33] K. Zyczkowski, P. Horodecki, A. Sanpera, and M. Lewenstein, Phys. Rev. A **58**, 883 (1998).
- [34] A. G. White, D. F. V. James, W. J. Munro, and P. G. Kwiat, Phys. Rev. A **65**, 12301 (2001).
- [35] H. S. Eisenberg et al., Phys. Rev. Lett. **93**, 193901 (2004).